Title

Radiation dose estimation for pencil beam X-ray luminescence computed tomography imaging.

Journal

Journal of X-Ray Science and Technology, 29(5)

ISSN

0895-3996

Authors

Romero, Ignacio O

Li, Changqing

Publication Date

2021

DOI

10.3233/xst-210904

Peer reviewed

Radiation dose estimation for pencil beam x-ray luminescence computed tomography imaging

Ignacio O. Romero, and Changqing Li*

Department of Bioengineering, University of California, Merced, Merced, CA, USA.

*Corresponding Author: Changqing Li, Email: cli32@ucmerced.edu

Abstract

Background: Pencil beam x-ray luminescence computed tomography (XLCT) imaging provides superior spatial resolution than other imaging geometries like sheet beam and cone beam geometries. However, the pencil beam geometry suffers from long scan times, resulting in concerns over dose which discourages the use of pencil beam XLCT.

Objective: The dose deposited in pencil beam XLCT imaging was investigated to estimate the dose from one angular projection scan with three different x-ray sources. The dose deposited in a typical small animal XLCT imaging was investigated.

Methods: A Monte Carlo simulation platform, GATE (Geant4 Application for Tomographic Emission) was used to estimate the dose from one angular projection scan of a mouse leg model with three different x-ray sources. Dose estimations from a six angular projection scan by the three different x-ray source energies were performed in GATE on a mouse trunk model composed of muscle, spine bone, and a tumor.

Results: With the Sigray source, the bone marrow of the mouse leg was estimated to have a radiation dose of 44 mGy for a typical XLCT imaging with six angular projections, a scan step

size of 100 micrometers, and 10^6 x-ray photons per linear scan. With the Sigray x-ray source and the typical XLCT scanning parameters, we estimated the dose of the spine bone, muscle tissues, and tumor structures of the mouse trunk were 38.49 mGy, 15.07 mGy, and 16.87 mGy, respectively.

Conclusion: Our results indicate that an x-ray benchtop source (like the x-ray source from Sigray Inc.) with high brilliance and quasi-monochromatic properties can reduce dose concerns with the pencil beam geometry. The findings of this work can be applicable to other imaging modalities like x-ray fluorescence computed tomography if the imaging protocol consists of the pencil beam geometry.

Keywords: x-ray luminescence computed tomography, x-ray imaging, radiation dose, GATE, Geant4

1. Introduction

X-ray luminescence computed tomography (XLCT) has emerged as a promising molecular imaging tool because XLCT combines the high measurement sensitivity of optical imaging and high spatial resolution of x-ray imaging. XLCT uses x-ray beams to excite nanophosphors embedded in deep tissues of the imaging object. The nanophosphors emit optical photons to be measured for optical imaging. The width and position of the pencil beam can be used as structural guidance to reconstruct the XLCT image therefore creating a molecular image with high spatial resolution [1-3]. A schematic of the XLCT imaging principle is shown in Fig. 1. Pencil beam XLCT imaging provides superior spatial resolution than other XLCT geometries like sheet beam and cone beam geometries because the fine pencil beam can provide anatomical guidance in the XLCT image reconstruction to resolve fine targets. The structural guidance information is lost when using the sheet beam and cone beam geometries for XLCT imaging which limit the sensitivity and spatial resolution [4, 5-8]. However, a pencil beam scan suffers from long scan times. Thus, concerns with dose discourage laboratory use of pencil beam x-ray sources. To minimize the dose, benchtop x-ray sources are filtered to remove the lower energy x-ray photons, but the added filtration increases the scan times.

In this work, the dose deposited into a small object (5 mm in diameter) using a pencil x-ray beam geometry was simulated in GATE (Geant4 Application for Tomographic Emission) [9]. The small object was composed of water, bone and blood to simulate the bone marrow structures of a mouse leg. Three different x-ray sources were simulated, and the dose and dose rate delivered from one angular projection scan were shown and compared. The dose measurements were repeated with different x-ray output rates to generate the linear relationship of the absorbed dose in each structure to the x-ray source output photon number. Among the three different x-ray

sources, a benchtop quasi-monochromatic x-ray source from Sigray Inc was modeled. Next, a small (~30 mm in diameter) mouse trunk model composed of muscle, bone, and a breast malignant tumor was imported into GATE to estimate the total dose delivered in a six angular projection scan. The three different x-ray sources were simulated, and the dose and dose rate delivered to the different mouse structures are shown and compared.

The paper is organized as follows. In section 2, the methods of the GATE simulations, setup, and source spectra are presented. In section 3, the results showing the relationships between x-rays output and dose with different spectra are presented. The paper concludes with discussions of the results and future works.

2. Methods

2.1 GATE programming

The GATE software was developed by the international OpenGATE collaboration as a GEANT4 wrapper that encapsulates the GEANT4 libraries specific to medical imaging and radiotherapy [9]. GATE utilizes the macro language to ease the learning curve of GEANT4 and allow GEANT4 toolkits to be more accessible to medical imaging and radiotherapy researchers [9]. GATE has now allowed for the design and optimization of new medical imaging devices and radiotherapy protocols [9, 10].

The GATE simulations in this work were parallelized and executed with a custom bash script on a 20 CPU workstation. The Penelope physics package (empenelope) from GEANT4 was used to model the physical processes. The Dose Actor feature from GATE was used to store the dose delivered to the volume inside a 3D matrix [10].

2.2 Bone marrow phantom setup

A 5 mm diameter cylindrical water phantom with a 2 mm diameter cylindrical bone structure located at the phantom center was simulated in GATE. A 1 mm diameter cylindrical blood structure was centered in the bone structure to simulate the bone marrow. The imaging object was placed at the center of the reference axis. The source beam width at the central coronal slice (x-axis) was 100 μm. A linear scan step size of 100 μm was used to acquire a single angular projection. The schematic of the bone marrow phantom GATE simulation setup along with a snapshot of the GATE simulation is shown in Fig. 2. The black box in the schematic is a representation of the dose actor tool from GATE which is seen as the white framed box around the simulated object.

The dose was stored in a 5 mm^3 cube with voxel size of 0.1 mm^3. 5×10^5, 7.5×10^5, 10^6, 1.25×10^6 and 1.5×10^6 x-ray photons were used for each linear scan step to establish a linear relationship between x-ray photon number and dose. From the linear relationship, the dose delivered by the x-ray sources at any output rate can be estimated by linear interpolation.

2.3 Mouse model setup

A 32.6 mm diameter mouse trunk model was simulated in GATE. To generate the mouse model, a mouse CT image from a previous microCT scan was processed in MATLAB to show only the muscle and the spine of the mouse. The mouse trunk CT image is shown in Fig. 3a. A 6.2 mm diameter tumor composed of 8%wt calcium oxalate was simulated and positioned close to the spine of the mouse model as shown in Fig. 3b. Calcium oxalate has been found to exist at higher concentrations in malignant breast tissues [11, 12]. Breast cancers are commonly used in mouse tumor models [13, 14]. A schematic of the GATE simulation with the mouse model is shown in

Fig. 3b. The mouse model was discretized into 186×176×1 voxels. The voxel size was set to 0.2 mm^3. The mouse model was placed at the center of the reference axis. The source beam width at the central coronal slice (x-axis) was 100 μm. A linear scan step size of 100 μm with 380 linear steps per angular projection and six angular projections with an angular step size of 30° was used to scan the mouse (0°, 30°, 60°, 90°, 120°, 150°).

The dose deposited in the mouse model was stored in a 186×176×1 cube with voxel size of 0.2 mm^3. 5×10^5, 6.25×10^5, 7.5×10^5, 8.75×10^5, and 10^6 x-ray photons were used for each linear scan step to generate the linear relationship between the x-ray photon number and dose. From the linear relationship, the dose delivered by the x-ray sources to each mouse structure at any output rate can be estimated by linear interpolation.

2.4 X-ray source spectra modeling in GATE

For the x-ray source from Sigray Inc., we have estimated and plotted its energy spectrum in Fig. 4. To simulate the XOS x-ray source (X-Beam Powerflux [Mo anode], XOS) in our lab, a 50 kVp spectrum of the x-ray source with polycapillary lens was acquired and normalized. The polycapillary lens only focused x-ray photons with energies less than 30 keV. The lab x-ray tube focuses x-rays to an approximate focal spot size of 100 μm at its focal distance. The histogram user spectrum tool from GATE was used to import the XOS source histogram. The energy of the emitted photon within each bin of the histogram was distributed uniformly. The spectrum is plotted in Fig. 5a below. Due to the utilization of a polycapillary lens, the spectrum was truncated after 30 keV. To minimize the dose contribution from low energy x-ray photons, a 2 mm Al filter was positioned in front of the source. The spectrum for the filtered XOS lab source was calculated and plotted in Fig. 5b.

2.5 Dose estimations

The dose stored in each voxel in GATE was calculated as the energy deposited per mass of the voxel. For the water phantom, the dose for bone marrow, bone, and object background were calculated as the mean dose from each region. This was done by using masks to identify only those pixels belonging to the bone marrow, bone, or object background and then the values in each region were averaged. For the mouse trunk model, the dose for the bone, muscle, and tumor were calculated as the mean dose from each structure. This was done by using masks to identify only those pixels belonging to the bone, muscle, or tumor. Then the values in each structure were averaged. All dose calculations were done in MATLAB after the GATE simulations had been completed.

3 Results

3.1 Results of the bone marrow dose map in one projection XLCT imaging

Fig. 6 shows the central line profile and dose maps for the cases of the filtered XOS source, unfiltered XOS source, and Sigray source. All the sources had an x-ray photon number of 10^6 per linear scan step. All three cases had 50 linear steps with the same pencil beam size and step size of 100 micrometers. From Fig. 6, it is shown that the bone structure absorbed more dose than the surrounding background and bone marrow structures due to the bone's greater effective atomic number (Z). In Fig. 6a, the addition of the Al filter results in the removal of the high entrance dose as seen in Fig. 6b. Without the Al filter, the lower energy photons result in increased air ionizations and superficial dose which result in the high entrance dose as seen in the central slice line profile and dose map of Fig. 6b. However, by adding a filter, the mean energy of the x-ray source is

increased which results in beam hardening and the x-rays become more penetrating to deliver greater dose in deeper structures. This can be seen by the increased dose in the right bone peak and the exit dose of the central slice line profiles in Fig. 6a compared to those in Fig. 6b. The shadowing effects are also less severe as shown in Fig. 6a due to the beam hardening effects. Fig. 6c shows more uniformity in the dose distribution due to a greater average energy by the Sigray source and less dose in the bone morrow region compared with the XOS source cases.

3.2 Bone marrow dose estimation based on x-ray photon number for one projection XLCT imaging

Fig. 7 shows the regression line plots with trendline equations relating the x-ray number per linear scan step (photons/step) to the absorbed average dose (Avg Dose) in milliGray (mGy) units for cases of the filtered XOS source, the unfiltered XOS source, and the Sigray source and for the different components of the phantom. All regression plots showed a high positive linearity with all R^2 values being greater than 0.99. For all regression plots, the bone structure shows greater values of average absorbed dose than the bone marrow and background structures. All the trendlines equations for the bone structure show a greater slope therefore bone will absorb dose at a greater rate than the other structures. For Fig. 7a, the regression lines of bone marrow and background are identical. Fig. 7a shows a slight increase in the dose rate of the bone structure due to the beam hardening effects from the Al filter. In Fig. 7b, the background regression curve is greater than the bone marrow regression curve due to the bremsstrahlung energies depositing significant dose to the background. Fig. 7c shows the lowest absorbed dose rate for the bone structure. Fig. 7c also shows a decrease of at least a half order of magnitude in the absorbed dose rate in bone marrow and background structures.

3.3 Bone marrow dose estimation of a typical XLCT scan

As we reported in our XLCT imaging studies [15-17], only six angular projections are needed for the narrow beam based XLCT imaging. The x-ray tube output photon number in each linear scan step depends on many factors including the detector sensitivity, the x-ray excitable phosphor particle brightness, the linear scan speed, and the target size and depth, etc. Generally, it can be assumed that the x-ray photon number is about 10^6 per linear scan. For each angular projection, the radiation dose in bone marrow was calculated to be 7.301 mGy as indicated in Fig. 7c for the Sigray source case. For a typical XLCT scan with 6 angular projections, we estimate the bone marrow dose to be about 43.806 mGy.

3.4 Results of dose map for the mouse model in one projection XLCT imaging

Fig. 8 shows the central line dose profiles and dose maps from a single angular projection for the different x-ray sources. All the sources had an x-ray photon number of 10^6 per linear scan step. All three cases had 380 linear steps with the same pencil beam size and step size of 100 micrometers. From Fig. 8a and 8c, it is shown that the bone structure absorbed more dose than the other mouse structures which is consistent with the results from the small mouse leg in Fig. 6. In Fig. 8b, the bone received little dose due to the limited number of x-rays with enough energy to penetrate to deeper tissues. The majority of the dose is seen deposited along the surface of the mouse trunk with little to no dose deposited in deeper tissues due to the bremsstrahlung energies of the unfiltered XOS source. Fig. 8b also shows greater dose absorbed in air than Fig. 8a and 8c thus contributing to the dose along the surface of the mouse trunk. In Fig. 8a, greater shadowing effects are observed compared to Fig. 6a due to the greater size of the imaging object, therefore less dose is deposited in deeper tissues. With the addition of the Al filter, the mean energy of the

x-ray source is increased, and greater transmission is observed thus the superficial tissues of the mouse trunk are spared from dose. Fig. 8c shows little shadowing effects and more uniformity in the dose distribution due to a greater mean energy of the Sigray source.

3.5 Results of the mouse model dose map for a typical XLCT scan

Fig. 9 shows the total dose maps and central line profiles from six angular projections for the three different x-ray sources. All the sources had an x-ray photon number of 10^6 per linear scan step. All three cases had 380 linear steps with the same pencil beam size and step size of 100 micrometers per angular projection. Fig. 9a shows that the greatest accumulation of the dose is found at the superficial tissues and the dose falls at a moderate rate in deep tissues as seen in the line profile. In Fig. 9b, the greatest accumulation of the dose lies strictly on the surface of the mouse model with minimal dose extending to deeper tissues. The line profile of Fig. 9b shows the dose decreases at an exponential rate in deeper tissues. Due to the drastic dose falloff from the mouse model surface, the tumor and bone structures are not very noticeable in the dose map thus showing little absorbed dose compared to the dose in air. Fig. 9b also shows the greatest accumulated dose in air when compared with Fig. 9a and 9c which increases the surface dose of the mouse trunk. Fig. 9c shows a more uniform distribution of the dose compared to Fig. 9a and 9b so that the tumor and bone structures are clearly displayed in the dose map. The line profile from Fig. 9c shows a dose decrease that resembles a more linear rate. The dose to air in Fig. 9c is minimal compared to Fig. 9a and 9b. Our results indicate that the surface of the mouse model is spared from additional dose for the case with the Sigray source.

3.6 Mouse model dose estimation based on x-ray photon number for six projection XLCT imaging

Fig. 10 shows the regression line plots relating the x-ray number per linear scan step (photons/step) to the absorbed average dose (Avg Dose) in milliGray (mGy) units for cases of the filtered XOS source, the unfiltered XOS source, and the Sigray source and for the different components of the mouse model after six angular projections. All regression plots showed a high positive linearity with all R^2 values being greater than 0.97. For the filtered XOS and Sigray source regression plots, the bone structure shows greater values of average absorbed dose than the muscle tissues and tumor. Due to the limited penetrability of the unfiltered XOS source, the muscle tissues show the greatest values for average absorbed dose when compared to the bone and tumor structures as seen in Fig. 10b. From Fig. 10, the dose rate for the muscle tissues was the lowest with the Sigray source. The dose rate for the tumor and bone were lowest with the unfiltered XOS source, however, this was due to the low penetrability of the source x-ray photons as seen in Fig. 9.

Table 1 shows the dose deposited in the spine bone, muscle tissues, and tumor structures of the mouse model by each source spectra after six angular projections with 10^6 x-ray photons/step. Table 1 also shows the dose deposited for the whole mouse model. The muscle tissues absorbed the least amount of dose with the Sigray source. The spine bone and the tumor structures absorbed the least amount of dose with the Unfiltered XOS. The whole body of the mouse model absorbed the least dose with the Sigray source. The filtered XOS source was responsible for the greatest dose delivered to all mouse model structures.

4. Discussions and Conclusions

In this work, the dose deposited into a 5 mm diameter mouse leg model by one projection pencil beam x-ray imaging was simulated in GATE. Then the dose deposited into a 32 mm

diameter mouse model by six projection pencil beam x-ray imaging was simulated. The dose deposited in both models by three different x-ray source spectra was shown and compared. The removal of bremsstrahlung energies results in decreased superficial dose thus making the filtered XOS source or the Sigray source a better choice for imaging. However, in a practical setting, a source filter will add to the imaging protocol.

Higher mean x-ray energies were observed to give greater dose in deeper depths due to the beam hardening effects. This effect was observed when comparing the unfiltered XOS source to the filtered XOS source results. With the filtered XOS source, the bone structures and bone marrow had greater dose rate as seen in the regression plot in Fig. 7. X-rays become less susceptible to the photoelectric effect at greater energies therefore the x-rays may be fully absorbed at greater depths which explains the greater background dose and bone dose with the filtered XOS source in the mouse leg model. In the mouse trunk model, this can be observed in the one projection scan.

Due to the size of the imaging objects, the Compton scattering dose effects are minimal compared to the photoelectric effect. However, the photoelectric effect is inversely related to the energy of the x-ray. Therefore, at much greater energies, x-ray transmission is more likely to occur. In the bone marrow model, this explains why the filtered XOS source shows greater dose and dose rates for all structures than the Sigray source. In the mouse model, the greatest absorbed dose for all structures was delivered with the filtered XOS source as seen in Table 1. From Fig. 4 and Fig 5, the average energy of the filtered XOS source is lower than the Sigray source, therefore the filtered XOS source is more susceptible to the photoelectric effect which increases the dose of the object tissues. The Sigray source would be a great alternative to other lab sources (like XOS) in XLCT imaging.

For a typical XLCT imaging scan with the Sigray source, more transmitted x-rays will be absorbed to excite the phosphor contrast agents while the surrounding tissues are spared from dose. From Fig. 9c, the entirety of the mouse trunk absorbed dose to relative levels unlike Fig. 9a and Fig 9b which showed great disparities between the surface and deep tissues. This means that good imaging can be acquired with the Sigray source without concerns of the starting imaging object position and with little concerns of absorbed dose. If a relatively longer scan is required to collect a better phosphor signal, the dose rates for muscle tissues were shown to be minimal when using the Sigray source as seen in Fig 10. With the XOS sources, the dose rates are dependent on the starting positions of the imaging object since the source x-ray energies are not as penetrating as the Sigray source. If the mouse model was to have rotated the opposite direction, the dose rates for the bone and tumor with the XOS sources would be much greater than the Sigray source.

XLCT uses x-rays to excite x-ray excitable nanoparticles embedded deep in tissues. The emitted optical photons are collected to reconstruct the image at a good resolution by using the x-ray beam positions as anatomical guidance in the XLCT reconstruction. Unlike XLCT, optical luminescence or fluorescence imaging use low energy optical photons to excite contrast agents and suffer from strong optical scattering in deep tissues that limits the image spatial resolution and the imaging depth. X-ray luminescence imaging offers only 2D imaging of the object while XLCT can offer volumetric imaging of the object if the object is scanned slice by slice.

The dose maps give a distribution of the deposited energy which is good information to know when using nanoparticles in XLCT imaging since the nanoparticles require energy for excitation to emit the optical photons. With the imaging scheme of six angular projections with 100 μm step size and 10^6 x-rays/step, the average accumulated dose was 15.42 mGy if using the Sigray source. Our lab has experimentally measured the accumulated dose of a small phantom

object (~25 mm diameter) after six angular projections from an XOS source (~68.6 mGy) [15]. The dose measurements in this work are within the safety levels of a typical small animal micro-CT scan in which the dose from a scan with 600 projections is >200 mGy [18]. One can estimate the deposited dose in XLCT imaging after considering the effects of projection numbers, imaging time, and x-ray tube currents based on our simulated dose distributions. Furthermore, the dose calculation can be applied for cancer theranostics (like x-ray luminescence induced photodynamic therapy).

In summary, dose measurements were first performed on a 5 mm diameter object size, and then performed on a 32 mm diameter mouse model with three different pencil beam x-ray spectra. This work provides insight to the concerns associated with XLCT imaging with a pencil beam geometry. With an adequate x-ray benchtop source with high brilliance and quasi-monochromatic properties like the Sigray source, the dose concerns can be reduced. With the Sigray source, the bone marrow in the mouse leg model was estimated to have a radiation dose of 44 mGy for a typical XLCT imaging with six angular projections and 100 micrometer scan step size and 10^6 x-ray photons per linear scan. With the Sigray source, the spine bone, muscle tissues, and tumor structures of the mouse model received a radiation dose of 38.49 mGy, 15.07 mGy, and 16.87 mGy, respectively. The findings of this work will also be beneficial to other molecular x-ray imaging modalities like x-ray fluorescence computed tomography if it relies on a pencil x-ray beam imaging geometry.

Acknowledgements

This work was funded by the NIH National Institute of Biomedical Imaging and Bioengineering (NIBIB) [R01EB026646]. The authors thank Sigray, Inc. for providing the spectral information of the Sigray x-ray source.

5. References

[1] Li, C., Martínez-Dávalos, A., & Cherry, S. R. (2014). Numerical simulation of x-ray luminescence optical tomography for small-animal imaging. *Journal of Biomedical Optics*, *19*(4), 046002.

[2] Pratx G, Carpenter CM, Sun C, Xing L. X-ray luminescence computed tomography via selective excitation: A feasibility study. *IEEE Trans Med Imaging*. 2010;29(12):1992-1999

[3] Zhang W, Romero IO, Li C. Time domain X-ray luminescence computed tomography: numerical simulations. *Biomed Opt Express*. 2019;10(1):372-383

[4] Ahmad M, Pratx G, Bazalova M, Xing L. X-ray luminescence and X-ray fluorescence computed tomography: New molecular imaging modalities. *IEEE Access*. 2014;2:1051-1061

[5] Chen D, Zhu S, Chen X, et al. Quantitative cone beam X-ray luminescence tomography/X-ray computed tomography imaging. *Appl Phys Lett*. 2014;105(19)

[6] Liu X, Liao Q, Wang H. In vivo x-ray luminescence tomographic imaging with single-view data. *Opt Lett*. 2013;38(22):4530-4533

[7] Liu T, Rong J, Gao P, Zhang W, Liu W. Cone-beam x-ray luminescence computed tomography based on x-ray absorption dosage. *J Biomed Opt*. 2018;23(02):1-11

[8] Chen D, Zhu S, Cao X, Zhao F, Liang J. X-ray luminescence computed tomography imaging based on X-ray distribution model and adaptively split Bregman method. *Biomed Opt Express*. 2015;6(7):2649-2663

[9] Jan S, Santin G, Strul D, et al. GATE: a simulation toolkit for PET and SPECT. *Phys Med Biol*. 2004;49(19):4543-4561

[10] Sarrut D, Bardiès M, Boussion N, Freud N, Jan S, Létang J-M, Loudos G, Maigne L, Marcatili S, Mauxion T, Papadimitroulas P, Perrot Y, Pietrzyk U, Robert C, Schaart DR, Visvikis D, Buvat I. A review of the use and potential of the GATE Monte Carlo simulation code for radiation therapy and dosimetry applications: GATE for dosimetry. *Med Phys*. 2014 May 12;41(6):064301.

[11] Castellaro AM, Tonda A, Cejas HH, et al. Oxalate induces breast cancer. *BMC Cancer*. 2015;15(1):1

[12] Warren LM, Mackenzie A, Dance DR, Young KC. Comparison of the x-ray attenuation properties of breast calcifications, aluminium, hydroxyapatite and calcium oxalate. *Phys Med Biol*. 2013;58(7):N103-13

[13] Sakamoto K, Schmidt JW, Wagner KU. Mouse models of breast cancer. *Methods Mol Biol*. 2015;1267:47-71

[14] Park MK, Lee CH, Lee H. Mouse models of breast cancer in preclinical research. *Lab Anim Res*. 2018;34(4):160-165

[15] Zhang W, Lun MC, Nguyen AA, Li C. X-ray luminescence computed tomography using a focused x-ray beam. *J Biomed Opt*. 2017 Nov;22(11):1-11

[16] Zhang W, Zhu DW, Lun M, Li CQ. Collimated superfine x-ray beam based x-ray luminescence computed tomography. *Journal of X-ray Science and Technology*. 2017;25(6):945-957

[17] Zhang YM, Lun M, Li CQ, Zhou ZX. Method for improving the spatial resolution of narrow x-ray beam-based x-ray luminescence computed tomography imaging. *Journal of Biomedical Optics.* 2019;24(8):1-11.

[18] Boone, J.M., Velazquez, O., Cherry, S.R. Small-Animal X-ray Dose from Micro-CT. *Molecular Imaging*. 2004;3(3)

FIGURES

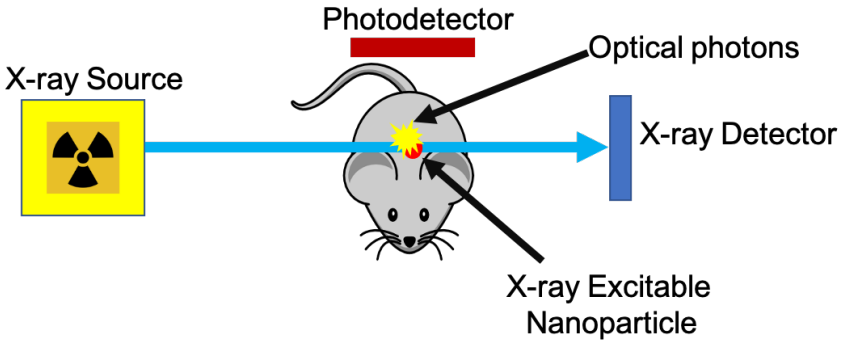

Fig. 1: Schematic of the x-ray luminescence computed tomography (XLCT) imaging principle.

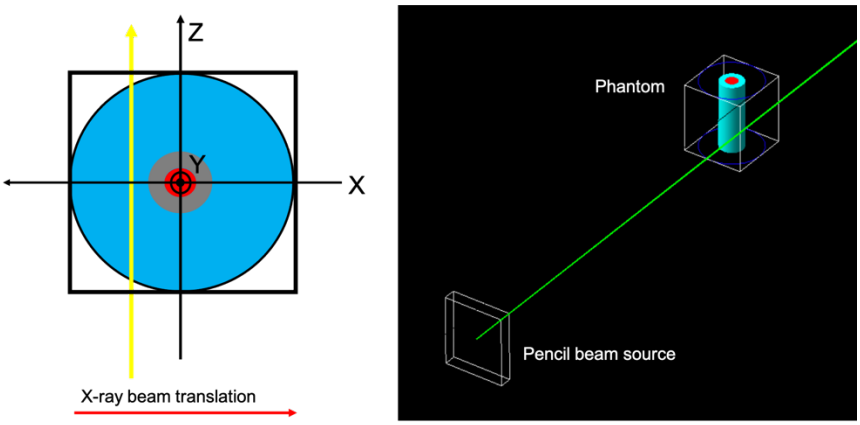

Fig. 2: Schematic (left) and simulation snapshot (right) of the pencil beam dose GATE simulations for the bone marrow study.

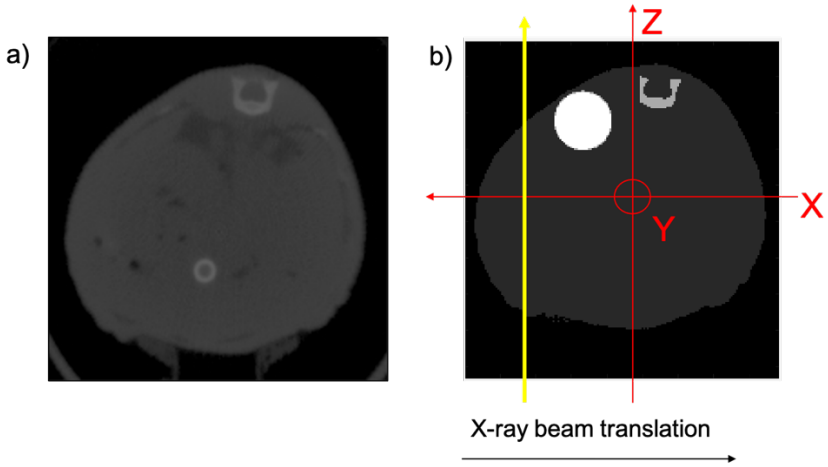

Fig. 3: a) A transverse slice of a mouse CT image; b) Schematic of the pencil beam GATE simulation with the mouse model. The difference in the image values in the mouse model is due to the different labeling values used for the GATE simulation.

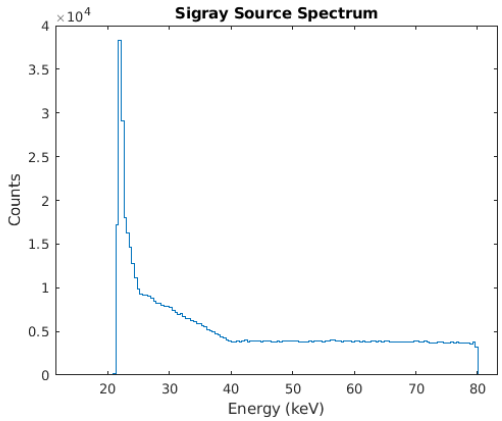

Fig. 4: The x-ray energy spectrum of the x-ray source from Sigray, Inc.

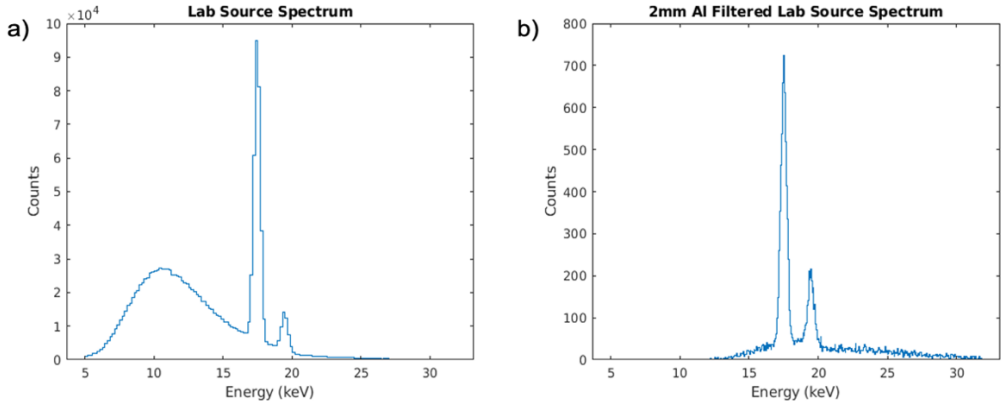

Fig. 5: The x-ray energy spectrum of the XOS source without (a) and with (b) a 2 mm thick aluminum filter after the polycapillary lens.

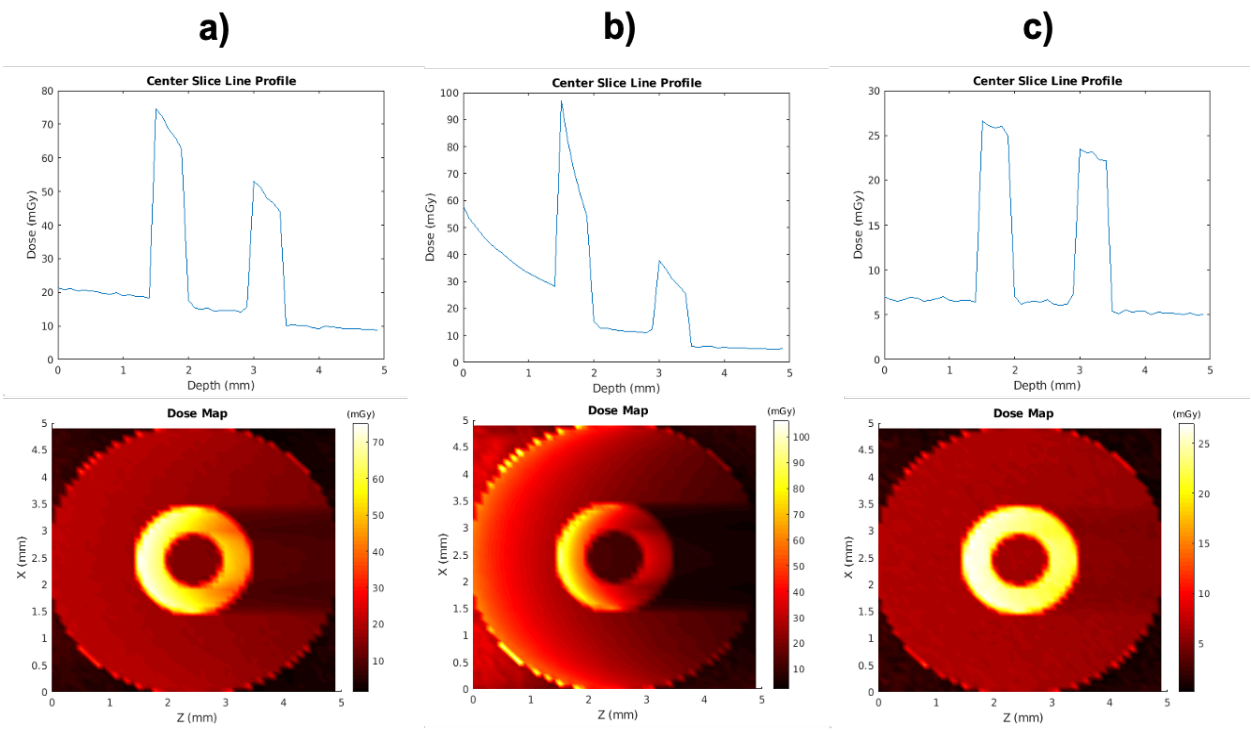

Fig. 6: Center slice line profile and dose maps of (a) Filtered XOS source, (b) Unfiltered XOS source, (c) Sigray source for 10^6 x-ray photons per linear scan step for all 50 steps.

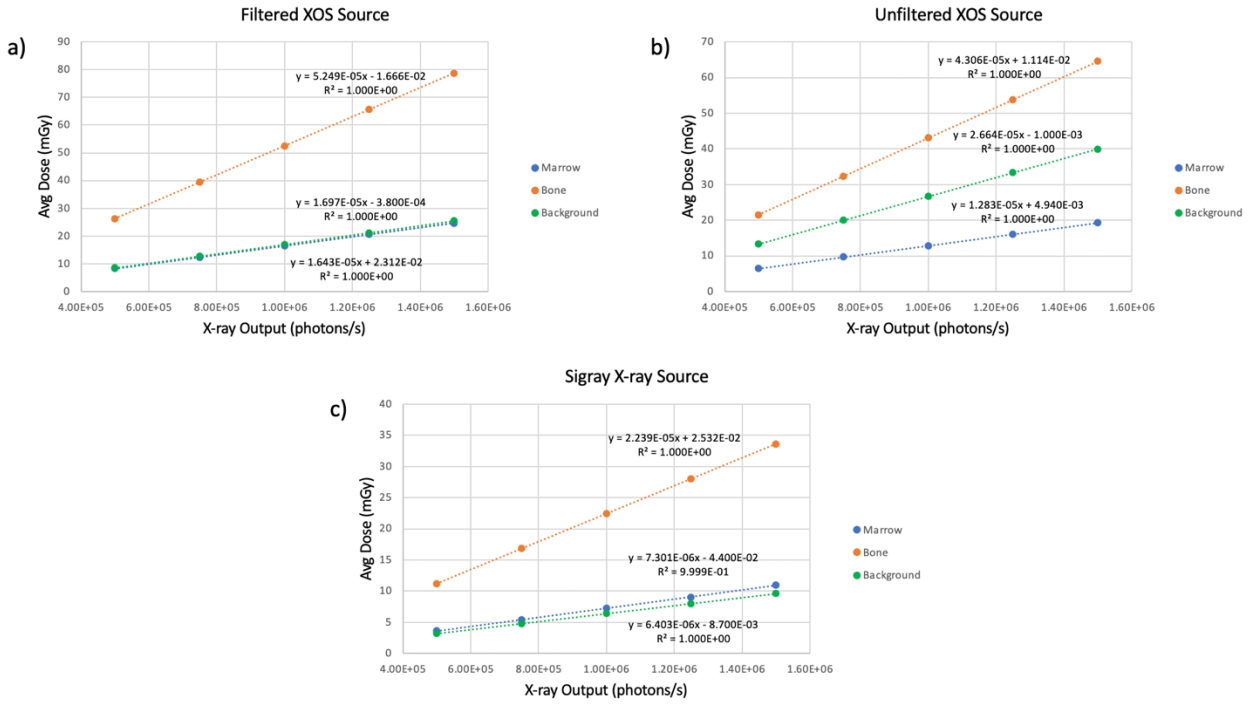

Fig. 7: Regression line plots of (a) filtered XOS source, (b) unfiltered XOS source, and (c) Sigray source for the different components of the phantom. In (a), the marrow and background plots are overlaid.

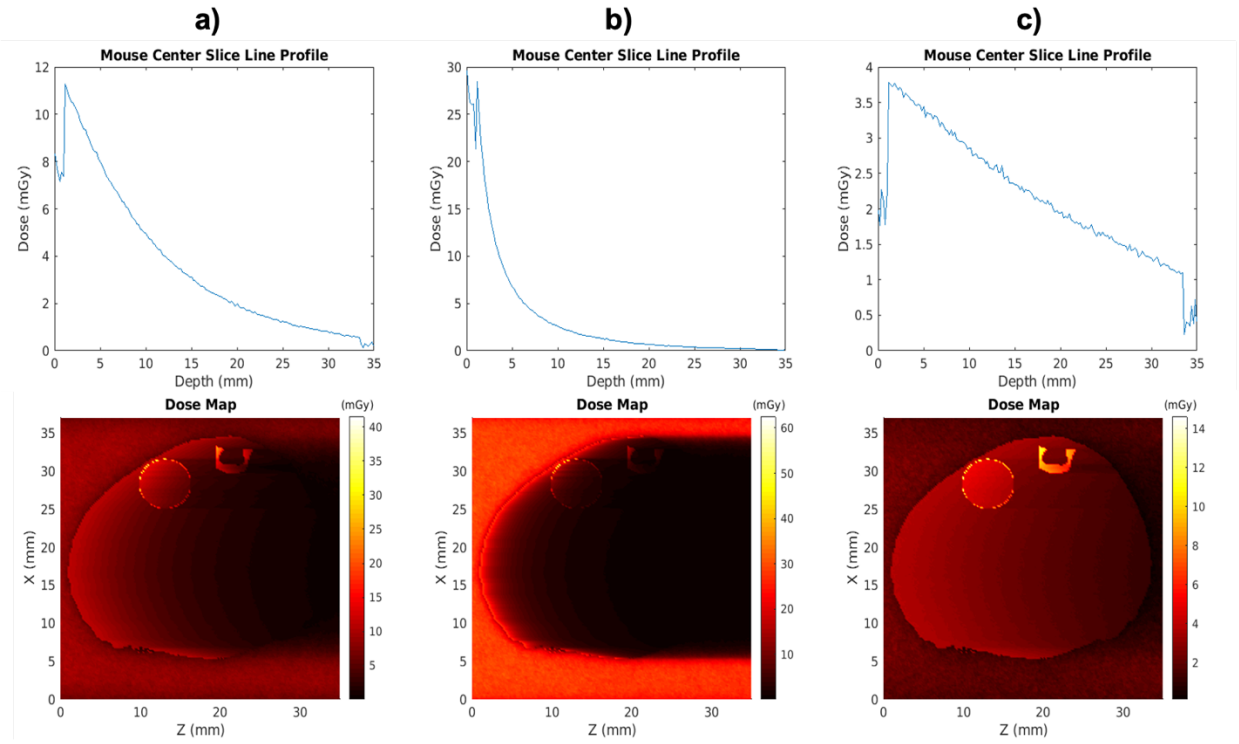

Fig. 8: Mouse model line profiles and dose maps of (a) Filtered XOS source, (b) Unfiltered XOS source, (c) Sigray source for 10^6 x-ray photons per linear scan step for one angular projection.

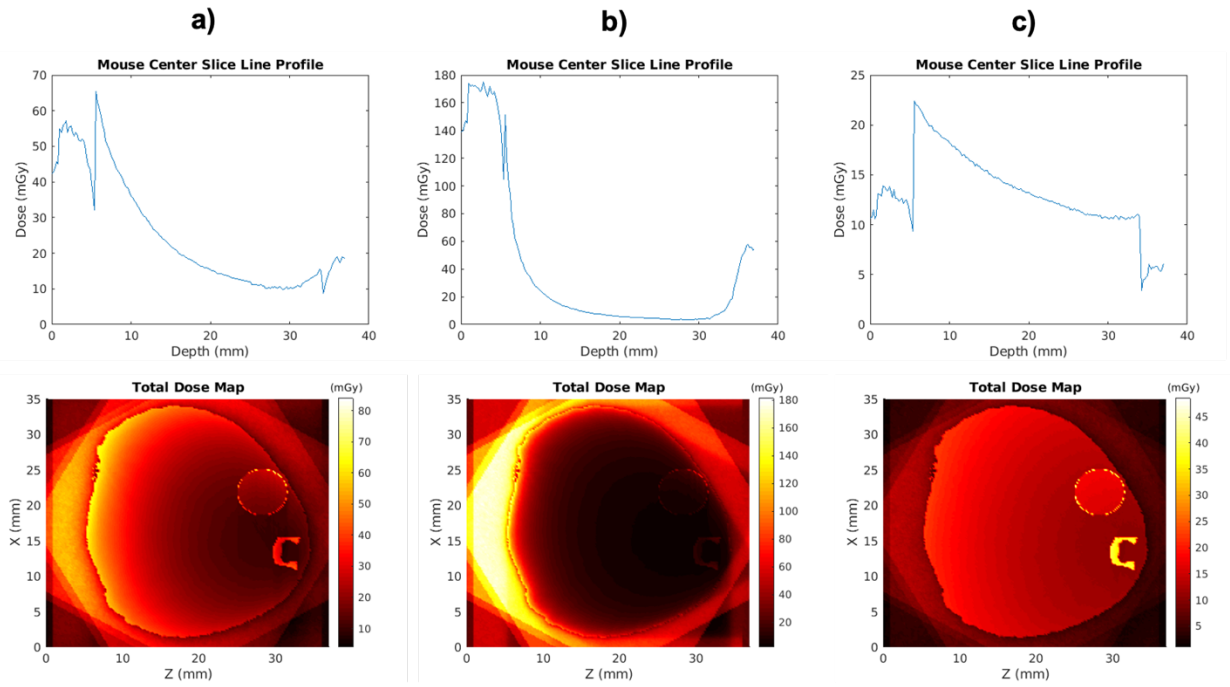

Fig. 9: Mouse model center slice line profile and total dose maps of (a) Filtered XOS source, (b) Unfiltered XOS source, (c) Sigray source for 10^6 x-ray photons per linear scan step after six angular projections with 30° angle step size.

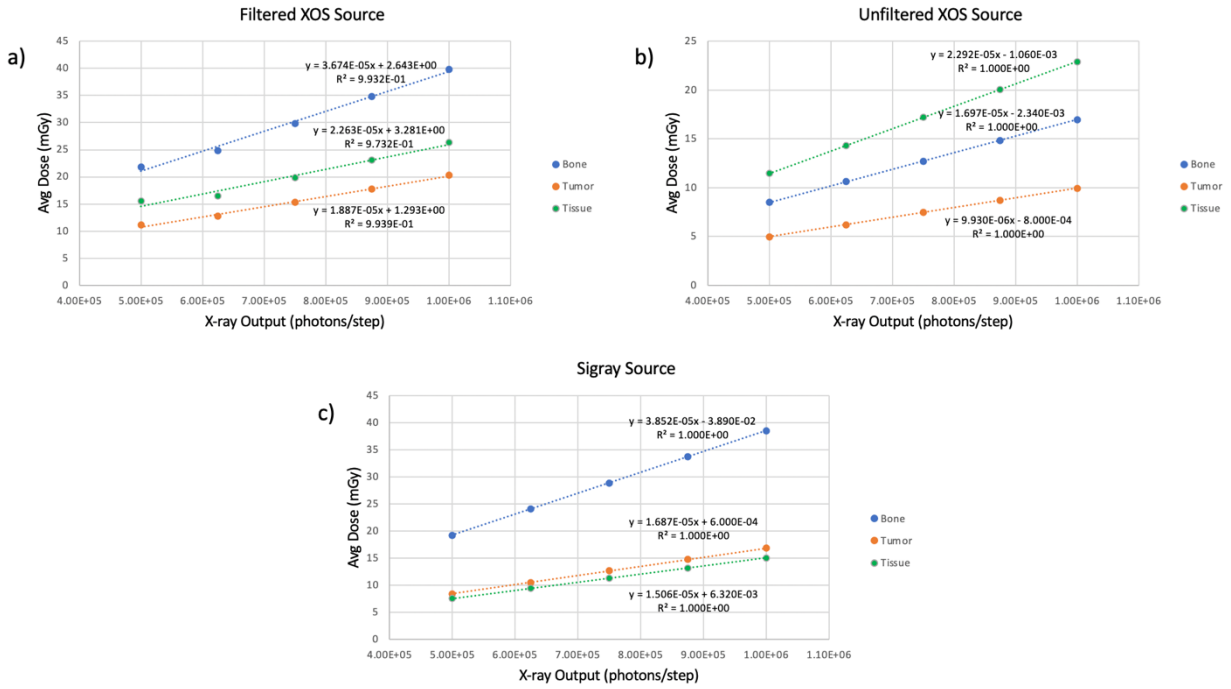

Fig. 10: Regression line plots of (a) filtered XOS source, (b) unfiltered XOS source, and (c) Sigray source for the different components of the mouse model after six angular projections.

TABLES

Table 1: Dose deposited in the mouse structures by each source spectra after six angular projections with 10^6 x-ray photons/step.

Model Structure	Dose by Filtered XOS	Dose by Unfiltered XOS	Dose by Sigray
Spine bone	39.77 mGy	16.97 mGy	38.49 mGy
Muscle Tissues	20.35 mGy	22.92 mGy	15.07 mGy
Tumor	26.38 mGy	9.93 mGy	16.87 mGy
Whole body	26.28 mGy	22.29 mGy	15.42 mGy